Published in final edited form as:
Circ Arrhythm Electrophysiol. 2020 October ; 13(10): e008249. doi:10.1161/CIRCEP.119.008249.

Optical Mapping-Validated Machine Learning Improves Atrial Fibrillation Driver Detection by Multi-Electrode Mapping

Alexander M. Zolotarev, MD[1,2], **Brian J. Hansen, PhD**[1], **Ekaterina A. Ivanova, MSc**[2], **Katelynn M. Helfrich, BSc**[1], **Ning Li, MD, PhD**[1,3], **Paul M.L. Janssen, PhD**[1,3], **Peter J. Mohler, PhD**[1,3], **Nahush A. Mokadam, MD**[3,4], **Bryan Whitson, MD, PhD**[3,4], **Maxim V. Fedorov, PhD**[2], **John D. Hummel, MD**[3,4,5], **Dmitry V. Dylov, PhD**[2,*], **Vadim V. Fedorov, PhD**[1,3,*]

[1]Dept of Physiology & Cell Biology & Bob and Corrine Frick Center for Heart Failure and Arrhythmia

[2]Center of Computational & Data-Intensive Science & Engineering, Skolkovo Institute of Science and Technology, Moscow, Russia

[3]Davis Heart & Lung Research Institute, The Ohio State University Wexner Medical Center, Columbus, OH

[4]Division of Cardiac Surgery, The Ohio State University Wexner Medical Center, Columbus, OH

[5]Dept of Internal Medicine; The Ohio State University Wexner Medical Center, Columbus, OH

Abstract

Background ––Atrial fibrillation (AF) can be maintained by localized intramural reentrant drivers. However, AF driver detection by clinical surface-only multi-electrode mapping (MEM) has relied on subjective interpretation of activation maps. We hypothesized that application of Machine Learning (ML) to electrogram frequency spectra may accurately automate driver detection by MEM and add some objectivity to the interpretation of MEM findings.

Methods ––Temporally and spatially stable single AF drivers were mapped simultaneously in explanted human atria (n=11) by subsurface near-infrared optical mapping (NIOM) (0.3mm^2 resolution) and 64-electrode MEM (Higher-Density (HD) or Lower-Density (LD) with 3mm^2 and 9mm^2 resolution, respectively). Unipolar MEM and NIOM recordings were processed by Fourier Transform analysis into 28407 total Fourier spectra. Thirty-five features for ML were extracted from each Fourier spectrum.

Results ––Targeted driver ablation and NIOM activation maps efficiently defined the center and periphery of AF driver preferential tracks and provided validated classifications for driver vs non-driver electrodes in MEM arrays. Compared to analysis of single electrogram frequency features, averaging the features for each surrounding 8 electrodes neighborhood, significantly improved classification of AF driver electrograms. The classification metrics increased when less strict annotation including driver periphery electrodes were added to driver center annotation. Notably, f1-score for the binary classification of HD catheter dataset were significantly higher than that of

---

Correspondence: Vadim V. Fedorov, PhD, Department of Physiology & Cell Biology, The Ohio State University Wexner Medical Center, 5196 Graves Hall, 333 W 10th Ave, Columbus, OH 43210-1218, Tel: 1-614-366-0986, vadim.fedorov@osumc.edu.

[*]contributed equally as co-senior authors

LD catheter (0.81 ± 0.02 vs 0.66 ± 0.04, $p<0.05$). The trained algorithm correctly highlighted 86% of driver regions with HD but only 80% with LD MEM arrays (81% for LD+HD arrays together).

Conclusions –– The ML model pre-trained on Fourier spectrum features allows efficient classification of electrograms recordings as AF driver or non-driver compared to the NIOM gold-standard. Future application of NIOM-validated ML approach may improve the accuracy of AF driver detection for targeted ablation treatment in patients.

Graphical abstract

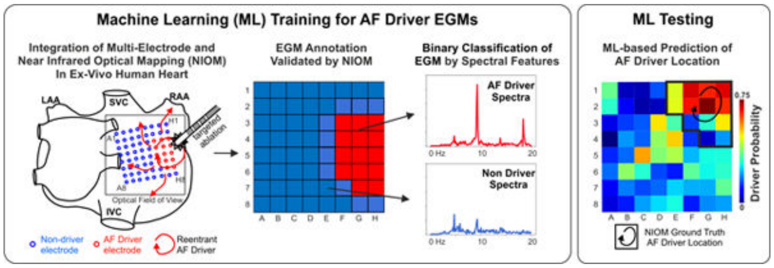

Keywords

Arrhythmias; Electrophysiology; Atrial Fibrillation; optical mapping; electrophysiology mapping; machine learning; multi-electrode mapping; targeted ablation

---

Introduction

Atrial fibrillation (AF) is the most common cardiac arrhythmia and the leading cause of stroke in the world.[1,23] The mechanism of this disease remains unclear, but several experimental and clinical studies suggest that AF may be caused and maintained by spatially-stable, extra-pulmonary sources of repetitive rotational activity called reentrant AF drivers.[4–6] Driver ablation can slow the rate of AF, convert it to atrial tachycardia, or terminate AF and restore sinus rhythm.[7] Unfortunately, clinical multi-electrode mapping (MEM) can record only the electrical signals from the atrial surface and may not detect the transmural conduction within the 3-dimensional structure of the human atria.[8,9]

One potential solution to improve AF treatment is related to the widespread adoption of Machine Learning (ML) techniques. In particular, several studies have applied machine and deep learning algorithms to classify ECG recordings into sinus rhythm, AF, and other arrhythmias.[10,11] ML has even been used to identify paroxysmal AF patients based on their sinus rhythm ECG.[12] In line with the goals of our own study, ML was used in-silico to identify the location of computationally simulated reentrant AF drivers [13]; however, many limitations have prevented translation of this work. Paramount among these limitations is the lack of a gold standard for AF driver detection in the clinical setting as clinical MEM is plagued by both false positives and false negatives.[8,14,15] Without a gold standard for validation, it would be impossible to correctly annotate the ML training set. Thus, an urgent need exists to develop a validated ML algorithm to improve AF driver detection for successful patient-specific AF ablation.

Our previous studies[4,8,16] have shown that these limitations in the visualization of reentrant AF drivers can be overcome in the ex-vivo human heart by high-resolution subsurface near-infrared optical mapping (NIOM) with submillimeter resolutions. We hypothesized that ML, verified by high-resolution NIOM, can efficiently distinguish MEM electrograms as originating from a reentrant AF driver or non-driver based on frequency features (e.g. the characteristics of the Fourier spectrum). Furthermore, since reentrant AF drivers cover an area greater than a single electrode, we explored if averaging the features across neighborhoods of electrodes could improve automated driver identification.

Methods

The data that support the findings of this study are available from the corresponding author upon reasonable request.

Explanted Human Hearts and Inclusion Criteria

Deidentified, coded human hearts were obtained from The Ohio State University Cardiac Transplant team (with left ventricular hypertrophy, ischemic and non-ischemic heart failure, atrial fibrillation, SND and comorbidities including chronic hypertension and diabetes) and LifeLine of Ohio (with and without arrhythmia history and comorbidities including hypertension, diabetes) in accordance with The Ohio State University Institutional Review Board. Clinical history of explanted hearts is shown in Supplementary Table I. Due to the focus of the study, only atrial preparations with sustained AF (>1min) and localized drivers confirmed by NIOM were included in this study's driver analysis. The following exclusion criteria were applied to ex-vivo human hearts with sustained AF: 1. Experiments where MEM did not efficiently cover NIOM-defined drivers (n=2). 2. Experiments with poor quality electrogram recordings (n=2). 3. Hearts (n= 3) with 2–3 NIOM-defined temporally competing, intermittent drivers observed during the 8–16 seconds recording. In total, 11 hearts had MEM grid driver coverage of a single NIOM-defined driver with temporal and spatial stability throughout the recording were used for the analysis.

Near-Infrared Optical Mapping of Coronary-Perfused Human Atria to Define AF Driver Regions

We employed high-resolution NIOM, the only approach currently able to reveal subsurface conduction in human atria and thus detect intramural AF driver activation as previously described[4,17,18]. Human atria were isolated, coronary-perfused, immobilized with blebbistatin (10 μM, Abcam), and stained with near-infrared voltage sensitive dye, di-4-ANBDQBS (10–40 μM, University of Connecticut Health Center). Ex-vivo panoramic and transmural NIOM employed three to four CMOS cameras (spatial resolution 0.3–1.1 mm, 1000 fps, MiCAM Ultima-L, SciMedia Ltd, CA), as previously described[4,8]. Biatrial (n = 6) and lateral right atrium (n=5) NIOM was conducted during sustained AF episodes to identify AF drivers as the ground truth with a MatLab program[4].

Induction of sustained AF by burst pacing was attempted in all hearts at baseline conditions in the absence of all pharmacologic stimulation. If AF was uninducible or spontaneously terminated, AF induction was then tested during mild pharmacologic challenge, as previously described[4,8,17] to represent autonomic tone or metabolic stress experienced by AF patients. Atria in which AF could not be sustained during mild pharmacologic challenge were excluded from the study. In 8 out of 11 experiments, targeted radiofrequency ablation was used to confirm the driver region as previously described[4,8](Figure 1). In 3 experimental procedures, ablation of driver sites was not performed due to technical issues with ablation delivery.

Multi-Electrode Mapping Electrograms

For simultaneous NIOM and clinically relevant MEM, two types of 64-electrode (8×8) catheter grids were used, provided by Abbott EP (Table 1). The Lower Density (LD) grid had an inter-electrode distance of 9 mm, 64-electrode FIRMap catheters (Abbott Labs, Chicago, Illinois) were customized and flattened so they could have ~7×7 cm^2 atrial surface coverage, as described previously[8]. The flattened LD catheter has the same electrode size ($1\times2mm^2$) and inter-electrode distances as its clinical counterpart the FIRMap catheter. The Higher Density (HD) grid had electrodes (1mm in diameter) made of the same gold-plated material as FIRMap catheters but with an inter-electrode distance of 3mm, and $22 \times 22mm^2$ surface coverage as described previously[19]. Unipolar electrograms were recorded from the LD or HD MEM with the indifferent electrode placed in the perfusion bath. The high pass filter was set at 0.05Hz and low pass filter at 500Hz with a 50Hz notch filter compared to a high pass filter of 30Hz and low pass filter of 500Hz for typical bipolar recording on the Ensite Velocity system (Abbott). The catheter grid was placed on the atrial tissue to cover the driver region indicated by the NIOM activation map (Figure 1). All recordings from HD grids were located within 2 cm to driver sites, but LD grids always contained EG recordings more than 2 cm away from the driver regions (~1×2cm) with their ~7×7 cm^2 coverage. Each recording was taken with the electrodes in a single position and point-by-point mapping was not used. Electrograms were recorded during the AF episodes using either LD (n =25) or HD (n =7) catheters simultaneously with NIOM optical action potentials (OAPs). The duration of the recordings varied from 8 to 16 seconds, as dictated by high-resolution four cameras NIOM recording system (a limitation of the high-resolution cameras).

Data Annotation Workflow

The ground truth for driver annotation was obtained similarly to the prior studies[4,8]. First, NIOM dominant frequency (DF, the frequency of the highest peak in the Fourier spectrum) was used to identify the fastest activating region, and then activation patterns based on the maximum derivative of NIOM OAPs were used to determine surface activation patterns within this region. As we previously published[4,8], intramural reentrant AF drivers could be identified at the surface with reentrant (>270° rotation), partial reentrant (>180° rotation), or focal (centrifugal activation) patterns. The preferential conduction paths of the AF drivers, as seen by NIOM, were used as the ground truth for electrode annotation. The preferential driver activation paths were defined independently by three reviewers and final reported annotation represents agreement among all three reviewers. Electrodes within one ablation lesion distance (~5mm) of the paths were defined as driver center electrodes (class 1) and electrodes outside of this distance threshold were defined as non-driver (class 0). Furthermore, non-diagonal adjacent electrodes were defined as driver periphery electrodes and were considered non-driver (class 0) in “driver center dataset” and driver (class 1) in "driver center plus periphery dataset". (Figure 1). Uninformative recordings (e.g., from electrodes with bad tissue contact) were annotated as outliers (class −1). Datasets were also labelled in accordance with the catheter resolution (Table 2). A simultaneously recorded NIOM OAP was manually selected within less than 1 mm adjacent to each electrode location for comparison.

Raw Signal Preprocessing

We applied signal normalization and 2–20 Hz Butterworth band-pass filtering to all recordings. MEM and NIOM recordings were then resampled into 5 second segments by a sliding window with 0.5 second steps (for Short-Time Fourier Transformation[20,21]). Fourier spectra were then calculated for each 5 second recording using a Fast Fourier Transform from NumPy library in Python (https://numpy.org/).

A set of frequency features for training a ML model was then generated from each Fourier spectrum, including DF listed as Frequency 1 among all other features in Table 3. The integer number n in the feature's name corresponds to the number of the n^{th} highest peak in the Fourier spectrum, ranging from $n = 1$ peak (the peak of DF) to n = 5 (the fifth highest peak). Spectral features *height*, *width*, *frequency*, and *prominence*, for each of the five highest peaks, were calculated using *scipy.signal* library in *Python*. An example of a MEM spectrum and the aforementioned features are shown in Figure 2A. Features *#peaks_0.05* and *#peaks_0.1* correspond to the number of peaks higher than a given threshold (5% and 10% of the height of the DF peak, respectively) to reflect values of noise present in the recordings. The peak-to-standard deviation ratio (PSDR) feature was calculated as the ratio between the average height of the two highest peaks to the standard deviation of heights across the whole spectrum. The other features are the ratios between features for each of the five tallest peaks.

For a given feature, each "*Neighborhood*" feature was then generated as a mean of the feature values of the 8 adjacent electrodes in a 3×3 grid, as visualized in Figure 2B. Examples of Fourier spectra from driver and non-driver neighborhood electrograms and OAPs are shown in Supplementary Figure I. The total number of generated features is equal to 35 for MEM feature sets.

Algorithm Selection and Testing

We tested 5 ML algorithms for binary classification: k-Nearest Neighbors (kNN), Support Vector Machine (SVM), Scalable Gradient Boosting (XGBoost), Random Forest (RF) and Logistic Regression (LR). The training/testing sets were randomly obtained from a 70%/30% split of the dataset, with each set having been stratified to provide the same balance of driver and non-driver recordings. Importantly, all windows from one electrogram were allocated to either the training or testing set.

In a subset analysis on driver prediction within the grid of a full MEM catheter recording, the training sets contained all recordings by a catheter (LD or HD), except for the 64 hold-out recordings from a single 8×8 catheter grid for testing. Recordings in the testing set labeled as uninformative were also excluded from the analysis. The algorithm then predicted the labels of each electrode M number of times, with M being equal to the number of the sliding windows from the data sampling step. The final probability of the electrode to be a driver is the mean of the probabilities of each sliding window to be a driver. We then visualized these probabilities as a heatmap, normalizing them from 0 (0% predicted driver probability) to 1 (100% predicted driver probability).

Performance Metrics

We used accuracy, precision, recall, f1-score and, area under the curve (AUC) for receiver operating characteristic (ROC) for each ML classification algorithm to evaluate its performance. Recall (or sensitivity) is the fraction of true positive driver electrodes selected by the algorithm among all possible driver electrodes. Precision (or positive predictive value) is the fraction of true positive drivers selected by the algorithm among all predicted drivers. AUC under ROC shows the prediction performance of the algorithm. f1-score is the harmonic mean of precision and recall, see the formula below.

ROC curve was used to select the best threshold for the binary classification between driver and non-driver recordings. The threshold was chosen to provide the best balance between recall and precision, and the best f1-score:

$$\text{fl-score}=\frac{2 \bullet \text{precision} \bullet \text{recall}}{\text{precision}+\text{recall}}.$$

The metrics for all datasets throughout the text are shown for the kNN algorithm, unless otherwise indicated, for the ease of reader interpretation. We investigated which features are the most valuable for the classification and how few features can be used without suffering a loss in f1-score. The subordinate features were removed until the value of f1-score dropped below the original confidence interval.

To carry out the feature importance analysis, we used an integrated *feature importance* function from the *XGBoost* library. The results were sorted in the descending order, with the most valuable feature being listed first and the relative contribution of the other features being normalized to the most valuable one.

To assess the possibility to identify the driver region within the whole grid, we calculated the averaged probability densities *per electrode* in the ground-truth location of the driver center plus periphery [D_{driver}] and in the background area outside of the driver (the non-driver region) [D_{outside}]. The quality of the prediction of the driver in a given part of the grid image (given the ground-truth annotation) is then optimally described by the driver contrast formula:

$$\text{Drivercontrast} = \frac{D_{\text{driver}} - D_{\text{outside}}}{D_{\text{driver}} + D_{\text{outside}}}$$

If the driver contrast is equal to 0, the prediction within the driver annotation mask is not distinguishable from any other regions; the higher the contrast is greater than 0, the easier it for a user to distinguish the driver region as the higher probability levels.

Statistical Analysis

Metrics are presented as *mean* ± *standard deviation*, calculated on 10 folds of the testing set. The performance of the binary classification on the reduced feature set is also reported as *mean* ± *confidence interval*. The analysis was done using the *scipy.stats* library in *Python*. Statistical significance between metrics on different options of feature sets for the same dataset or between metrics on different datasets was analyzed by Tukey's range test for pairwise samples or Repeated Measures ANOVA test for multifactor samples, with the *p*-value < 0.05 being considered as significant. The assumption of the metrics to be sampled from the normal distribution was verified using the Shapiro-Wilk test.

Results

Samples

The final dataset (LD+HD) consisted of 32 AF episodes in 11 explanted human atria with temporally and spatially stable AF drivers mapped by MEM and NIOM (Figure 1, Table 1). Each AF episode was mapped by a 64-electrode grid, resulting in a total of 32 × 64 = 2048 electrogram recordings. We expanded this number using data augmentation by Fourier transforming the windows of AF recordings, similarly to other works[20,22]. All data were later distributed into 2 datasets (LD or HD) based on catheter resolution.

Driver vs Non-Driver Classification

Amongst the 4 MEM frequency feature sets tested with the ML algorithm to classify MEM: single-electrode features of driver center annotation, single-electrode features of driver center plus periphery annotation, electrode-neighborhood features of driver center annotation and electrode-neighborhood features of driver center plus periphery annotation (for all n = 35 features); neighborhood electrodes of driver center plus periphery annotation performed best. The ROC curves of the 5 ML algorithms considered (kNN, SVM, XGBoost, RF and LR) for the AF LD+HD dataset are shown in Figure 3A. kNN accounting for 3 neighbors had the highest f1-score for the LD+HD dataset with driver center annotation, all 5 algorithms showed comparable f1-scores for driver center plus periphery annotation of LD +HD dataset. The performance metrics (accuracy, precision, recall, and f1-score) for the different feature sets and the highest f1-scores are presented in Figure 3B.

Performance of driver classification could be improved by averaging the features of eight surrounding neighborhood electrodes. Figure 3B shows that the values of metrics for the electrode-neighborhood feature set are all significantly higher than those for the single-electrode feature set. Similar dynamics were found for NIOM electrode-neighborhood feature set (Supplementary Figure II).

We also assessed how differences in catheter resolution could affect driver classification (Figure 4). Resolution was especially important for the electrode neighborhood dataset. Though the accuracy corresponding to the HD dataset was approximately equal to that for the LD dataset (89.2 ± 0.5% vs 89.3 ± 1.1% for driver center; 87.5 ± 0.1% vs 87.5 ± 0.2% for driver center plus periphery), other metrics were always higher for the HD dataset. The precision values ranged from 0.26 ± 0.05 for the LD MEM dataset of driver center annotation to 0.78 ± 0.03 for the HD MEM dataset of driver center plus periphery annotation. Furthermore, HD datasets had the highest recall and f1-score (0.84 ± 0.04 and 0.81 ± 0.02 for driver center plus periphery) while LD datasets had lower recall and f1-score (0.63 ± 0.05 and 0.66 ± 0.04 for driver center plus periphery). Moreover, Figures 3 and 4 show that regardless of catheter resolution the center plus periphery driver annotation always resulted in the highest performance metrics in comparison with driver center annotation. A full report on the metrics for all datasets predicted by the 5 ML algorithms can be found in Supplementary Table II.

Additionally, we tested how a pre-trained algorithm handles recordings without any driver electrodes in the vicinity, by placing the HD catheter remotely from the driver region. We tested 3 novel recordings of Heart #11 from the HD catheter after training on the AF LD +HD center+periphery neighborhood training set. The algorithm performed robustly in this task, yielding f1-score of 0.944 ± 0.003.

Feature Importance

The most valuable features for MEM are listed in Figure 5. The most valuable feature was the relative height (prominence) of the DF, with its frequency and the ratios between the DF height and heights of other peaks among the other most valuable features. The features that describe the noise in the spectrum (e.g., signal-to-noise ratio, number of peaks above a threshold, and prominence) were also found to play a vital role in the classification task. The order of the most valuable features slightly varied in different datasets (e.g., LD and HD datasets), as presented in Supplementary Figures III–IV. In addition, Supplementary Figure V shows the most valuable features for center vs center plus periphery annotation of LD +HD single-electrode dataset and Supplementary Figure VI shows an example of the distributions of features for Heart #8. Importantly, using only the single feature of electrode DF to predict AF driver electrodes had a precision of 0.31, a sensitivity of 0.26, and an f1-score of 0.28, which emphasizes the importance of our multi-feature ML based approach. We found that keeping only the 10 most valuable features (out of 35 MEM features) maintained an f1-score within the confidence interval of the full feature set.

Driver Localization on the Multi-Electrode Grid

Finally, we tested the ability of ML to highlight the location of the AF driver within a simultaneously recorded, clinically relevant 8×8 electrode grid by using the best classification dataset.

Figure 6 and Supplementary Figure VII show examples of driver probability heat maps for HD and LS catheter sets by all features and 10 most valuable driver features, respectively. The ML algorithm pre-trained on electrode neighborhoods and based on driver center plus periphery annotation correctly defined driver area as a region with the highest driver probabilities. Quantitatively, driver contrast from the background non-driver region demonstrates that the pre-trained algorithm can highlight the driver region for all three datasets with driver contrast higher than zero in 86% HD recordings and in 80% LD recordings. Complete results for all recordings are shown in the Supplementary Table III.

Discussion

We present here the first study in human hearts using ML approaches to predict the probability that MEM recordings originate from reentrant AF drivers based on extensive frequency characteristics. We investigated which features are the most valuable for driver classification. We observed that f1-score is significantly higher if electrode-neighborhood features are analyzed instead of single-electrode analysis; f1-score is significantly higher for center plus periphery driver annotation in contrast with center-only annotation; and f1-score for the HD dataset is higher than the LD dataset. We have also demonstrated the ability of the pre-trained ML algorithm validated by NIOM to define reentrant AF driver locations within clinically relevant electrode arrays.

Validation of AF Driver Location and Borders by NIOM Activation Maps

We validated the locations of reentrant AF drivers by NIOM, because NIOM can overcome the well-known limitations of MEM. NIOM can record signals over a depth of 4 mm, at a much higher resolution and does not require direct contact with the tissue[8]. Optical activation maps were able to clearly show driver activity at the driver site where targeted ablation terminated the AF episode (Figure 1), and thus provided validation of driver annotations. Importantly, no universal definition of AF drivers and their borders seen by MEM currently exist and current AF driver detection methods employed clinically are prone to both false positives and false negatives [8,14,15].

Our study shows a significant difference in classification metrics between center and center plus periphery driver annotation. Mechanistically, center plus periphery driver electrodes may cover the driver domain region that has predominantly one-to-one conduction with the driver. Thus, a “spill over” of features in the frequency domain may be present from preferential driver tracks to the immediately surrounding driver domain. As seen in Supplementary Figure IV, all features related to DF peak are less impactful for center annotation than for center plus periphery annotation. Further clinical and experimental studies will be necessary to hone more strict AF driver classification or possibly guide clinicians to the optimal ablation target within the driver domain.

Driver Temporal Stability and Plurality

In the current study, we used only AF recordings with single, temporally and spatially stable, NIOM-defined drivers to diminish uncertainty in the electrogram annotation for the training data set. However, the existence of several competing drivers in human AF is frequent. Our previous studies [23] showed that sustained AF in explanted human hearts may be maintained by two or more spatially stable, but temporally competing, reentrant drivers in both left and right atria. The presence of two or more spatially stable reentrant drivers within the human atria may allow these drivers to be temporally unstable or intermittent while permitting AF to be constantly maintained by at least 1 active driver. Furthermore, during ex-vivo human heart experiments where radiofrequency ablation successfully disrupted the track of the primary AF driver, a secondary slower AF driver could be unmasked in a different location, which would require subsequent mapping and targeted ablation.

Previous clinical[5,7,24] contact and non-contact[6] MEM studies as well as experimental NIOM[16,17] studies showed that AF can be maintained in patient-specific manner by either multiple competing recurring drivers or a single localized driver. Furthermore, in similar experimental ex-vivo human heart studies we recently revealed that due to limitations of the clinical MEM (surface only recordings) and the phase based analysis of clinical EG can simultaneously visualize more “false positive” drivers (~1.1 per AF visualization), during AF episodes vs true NIOM drivers confirmed by targeted ablation[8]. Thus, while we acknowledge the appearance of two or more simultaneous competing AF drivers may also result from the high false-positive rate of current clinical AF driver detection methods, as we previously reviewed[7]. Future studies must be done to test the effect of partial driver stability less than 5 seconds and the presence of multiple competing drivers on the predictive value of the ML algorithm.

Feature Selection

ML and deep learning approaches have begun to be used in the cardiovascular field[25,26]. We selected the ML approach because of the ‘black box’ problem of deep learning algorithms[27] and limited size of the current dataset. ML techniques are better suited for interpretable predictions when instead of relying on a set of abstract features generated by the machine, the mathematical model is purposely engineered using observable and handpicked, potentially meaningful characteristics of the signal. Unlike agnostic deep learning methods, we can clarify which features are valuable for the classification, in this case features of the frequency spectra of MEM. The ML algorithm appears to allow detection of subtle differences between the features originating from the driver and non-driver regions in the atria as measured by both MEM and NIOM.

Several clinical and animal studies show the importance of frequency characteristics in the task of AF driver detection[28–31], including instantaneous frequency calculations[32]. Unsurprisingly, it is the DF peak and its characteristics that hold the greatest classification power in detecting AF driver in the MEM (Figure 5) and NIOM (Supplementary Figure IV) feature datasets. This agrees with the previous work[8,28,30,33] where the features of AF drivers were studied. However, a number of studies show the inability of DF, the most common frequency of the signal, to be the sole feature for classification[14,34–36]. Our previous study showed that DF strongly correlated with AF driver regions on high-resolution NIOM maps, but MEM DF was not a specific driver feature[8]. Our current study also showed DF as the sole feature resulted in an f1-score of 0.28.

Instead, we observed that the frequencies, heights, and prominences of other highest peaks in the Fourier spectra, as well as the ratios between them, make important contributions to AF driver classifications by ML. Furthermore, several features of electrogram frequency spectra, aforementioned and noise-related such as PSDR or the number of peaks above some threshold, are critically important for distinguishing drivers from non-drivers. With these novel insights, future work could uncover how these features may inform driver mechanisms and the pathophysiology of the fibrillating heart. The list of all features sorted by their contribution (Figure 5) could be used to guide such future research. Moreover, we showed that if only the combination of the 10 most important features are used to highlight possible driver area, the locations of the highest driver probabilities remain in the same regions of the grid and still are inside the ground-truth driver region (Supplementary Figure VII). Although, contribution of each of these signal features should be validated in a separate clinical or pre-clinical study, the most important features are consistent with our current understanding about the mechanism of AF drivers.

Performance Metrics Depend on MEM Catheter Resolution

A ML model trained on single-electrode features performed below our expectations, leading us to consider the features calculated as an average of the electrodes within the surrounding neighborhood. The classifiers based on electrode-neighborhood features provide improved metrics for both MEM and NIOM data (Supplementary Figure II), which suggest the benefit of looking at AF drivers as a region instead of a single point, supported by the ~1.5 cm x 0.6 cm average area of reentrant AF drivers previously reported[16]. Importantly, f1-score, precision, and recall for the binary classification of HD catheter dataset were higher than the metrics of LD catheter dataset, emphasizing the importance of neighborhood resolution in driver classification. One of the reasons for these improvements could be that the average number of driver electrodes per recording was higher for HD compared to LD MEM arrays (10.9 ± 4.3 vs 4.0 ± 1.3). The distance between electrodes plays an important role in reentrant AF driver detection by MEM[37] as moderate resolution MEMs can miss a part of the driver reentrant track[7], with NIOM identifying reentrant tracks between and unmapped by widely spread electrode splines.

Traditionally, catheter resolution has been sacrificed for panoramic coverage of the atria, as sequential activation mapping with higher density grid is insufficient for driver detection during chaotic AF activation patterns[7]. The ML-based approach developed here could remove the need for activation mapping and allow the use of higher density catheters for improved AF driver identification. Specifically, this ML detection algorithm could be applied to sequential mapping, as long as each location will be mapped for at least 5 seconds. Alternatively, a panoramic LD catheter could be used first, and then an HD catheter moved to a region of interest for confirmation and better defining of the driver region.

Limitations

There are several limitations in our study. Findings from this small number of hearts with induced AF may not be representative amongst all persistent AF patients or mapping techniques. Moreover, the number of electrogram recordings were increased by sampling overlapping windows for the binary classification of the MEM recordings, which could introduce over fitting of the model. We used only recordings with stable single drivers in the current work to remove the variability in driver temporal stability from affecting electrogram annotation. We used only Fourier spectrum features for ML models training; other features of MEM electrogram analysis such phase mapping features and activation maps may also allow efficient classification of electrograms recordings as AF driver or non-driver and will be considered in future studies.

Conclusion

This pilot study has shown for the first time that a ML-based approach validated by high-resolution NIOM in human hearts can efficiently classify MEM electrograms as AF driver or non-driver by using the features from the Fourier spectra. This approach performed better when considering features from electrogram neighborhoods instead of single electrograms. The ML approach was also better at classifying electrodes at the driver center and its periphery than classifying the driver center alone. All types of classification performed better for recordings from HD MEM than LD MEM. Further application of the algorithm allowed prediction of AF driver location within electrode grids with modest 81% accuracy. Further validation of MEM recordings by NIOM and training with a larger dataset would improve future ML models to become complementary tools during clinical AF ablation procedures, bringing essential enhancement to conventional clinical MEM approaches to detect AF drivers.

Supplementary Material

Refer to Web version on PubMed Central for supplementary material.

Acknowledgments:

We thank the Lifeline of Ohio Organ Procurement Organization and the Division of Cardiac Surgery at The OSU Wexner Medical Center for providing the explanted hearts. The human heart program is supported by the Davis Heart and Lung Research Institute. We thank members of the Fedorov lab for their help with ex-vivo human atria mapping experiments.

Sources of Funding: National Institute of Health [grant numbers HL115580 and HL135109 to VVF, T32HL134616 and NIH F30HL142179 to BJH]; Russian Foundation for Basic Research [19–29-01240 “mk” to DVD]; and the Bob and Corrine Frick Center for Heart Failure and Arrhythmia.

Disclosures: Dr. Fedorov has received research support from Abbott. Dr. Hummel is a Consultant to Abbott. No other authors have declared competing interest.

Nonstandard Abbreviations and Acronyms

AF	Atrial Fibrillation
MEM	multi-electrode mapping
NIOM	near-infrared optical mapping
ML	Machine Learning
HD	Higher-Density
LD	Lower-Density
OAP	optical action potentials
DF	dominant frequency
PSDR	peak-to-standard deviation ratio
kNN	k-Nearest Neighbors

SVM	Support Vector Machine
XGBoost	Scalable Gradient Boosting
RF	Random Forest
LR	Logistic Regression
ROC-AUC	area under the curve for receiver operating characteristic

References:

1. Calkins H, Hindricks G, Cappato R, Kim YH, Saad EB, Aguinaga L, Akar JG, Badhwar V, Brugada J, Camm J, et al. 2017 HRS/EHRA/ECAS/APHRS/SOLAECE expert consensus statement on catheter and surgical ablation of atrial fibrillation: Executive summary. Europace. 2018;20:157–208. doi:10.1093/europace/eux275 [PubMed: 29016841]
2. Packer DL, Mark DB, Robb RA, Monahan KH, Bahnson TD, Poole JE, Noseworthy PA, Rosenberg YD, Jeffries N, Mitchell LB, et al. Effect of Catheter Ablation vs Antiarrhythmic Drug Therapy on Mortality, Stroke, Bleeding, and Cardiac Arrest Among Patients With Atrial Fibrillation: The CABANA Randomized Clinical Trial. JAMA. 2019;321:1261–1274. doi:10.1001/jama.2019.0693 [PubMed: 30874766]
3. Abideen AZU, Ali Y, Shahzeb KM, M A-KS, Stavros S. Catheter Ablation Versus Medical Therapy for Atrial Fibrillation. Circ Arrhythmia Electrophysiol. 2019;12:e007414. doi:10.1161/CIRCEP.119.007414
4. Hansen BJ, Zhao J, Csepe TA, Moore BT, Li N, Jayne LA, Kalyanasundaram A, Lim P, Bratasz A, Powell KA, et al. Atrial fibrillation driven by micro-anatomic intramural re-entry revealed by simultaneous sub-epicardial and sub-endocardial optical mapping in explanted human hearts. Eur Heart J. 2015;36:2390–2401. doi:10.1093/eurheartj/ehv233 [PubMed: 26059724]
5. Narayan SM, Krummen DE, Shivkumar K, Clopton P, Rappel W-J, Miller JM. Treatment of Atrial Fibrillation by the Ablation of Localized Sources: CONFIRM (Conventional Ablation for Atrial Fibrillation With or Without Focal Impulse and Rotor Modulation) Trial. J Am Coll Cardiol. 2012;60:628–636. doi:10.1016/J.JACC.2012.05.022 [PubMed: 22818076]
6. Haissaguerre M, Hocini M, Denis A, Shah AJ, Komatsu Y, Yamashita S, Daly M, Amraoui S, Zellerhoff S, Picat M-Q, et al. Driver domains in persistent atrial fibrillation. Circulation. 2014;130:530–538. doi:10.1161/CIRCULATIONAHA.113.005421 [PubMed: 25028391]
7. Hansen BJ, Csepe TA, Zhao J, Ignozzi AJ, Hummel JD, Fedorov V V. Maintenance of Atrial Fibrillation: Are Reentrant Drivers with Spatial Stability the Key? Circ Arrhythmia Electrophysiol. 2016;9:1–12. doi:10.1161/CIRCEP.116.004398
8. Hansen BJ, Zhao J, Li N, Zolotarev A, Zakharkin S, Wang Y, Atwal J, Kalyanasundaram A, Abudulwahed SH, Helfrich KM, et al. Human Atrial Fibrillation Drivers Resolved With Integrated Functional and Structural Imaging to Benefit Clinical Mapping. JACC Clin Electrophysiol. 2018;4:1501–1515. doi:10.1016/j.jacep.2018.08.024 [PubMed: 30573112]
9. de Groot N, van der Does L, Yaksh A, Lanters E, Teuwen C, Knops P, van de Woestijne P, Bekkers J, Kik C, Bogers A, et al. Direct Proof of Endo-Epicardial Asynchrony of the Atrial Wall During Atrial Fibrillation in Humans. Circ Arrhythmia Electrophysiol. 2016;9:e003648. doi:10.1161/CIRCEP.115.003648
10. Hannun AY, Rajpurkar P, Haghpanahi M, Tison GH, Bourn C, Turakhia MP, Ng AY. Cardiologist-level arrhythmia detection and classification in ambulatory electrocardiograms using a deep neural network. Nat Med. 2019;25:65–69. doi:10.1038/s41591-018-0268-3 [PubMed: 30617320]
11. Xiong Z, Nash MP, Cheng E, Fedorov V V, Stiles MK, Zhao J. ECG signal classification for the detection of cardiac arrhythmias using a convolutional recurrent neural network. Physiol Meas. 2018;39:94006. doi:10.1088/1361-6579/aad9ed
12. Attia ZI, Noseworthy PA, Lopez-Jimenez F, Asirvatham SJ, Deshmukh AJ, Gersh BJ, Carter RE, Yao X, Rabinstein AA, Erickson BJ, et al. An artificial intelligence-enabled ECG algorithm for the identification of patients with atrial fibrillation during sinus rhythm: a retrospective analysis of

outcome prediction. Lancet. 2019;394:861–867. doi:10.1016/S0140-6736(19)31721-0 [PubMed: 31378392]

13. McGillivray MF, Cheng W, Peters NS, Christensen K. Machine learning methods for locating re-entrant drivers from electrograms in a model of atrial fibrillation. R Soc Open Sci. 2018;5. doi:10.1098/rsos.172434
14. Benharash P, Buch E, Frank P, Share M, Tung R, Shivkumar K, Mandapati R. Quantitative Analysis of Localized Sources Identified by Focal Impulse and Rotor Modulation Mapping in Atrial Fibrillation. Circ Arrhythmia Electrophysiol. 2015;8:554–561. doi:10.1161/CIRCEP.115.002721
15. Vijayakumar R, Vasireddi SK, Cuculich PS, Faddis MN, Rudy Y. Methodology Considerations in Phase Mapping of Human Cardiac Arrhythmias. Circ Arrhythmia Electrophysiol. 2016;9:e004409. doi:10.1161/CIRCEP.116.004409
16. Zhao J, Hansen BJ, Wang Y, Csepe TA, Sul L V, Tang A, Yuan Y, Li N, Bratasz A, Powell KA, et al. Three-dimensional Integrated Functional, Structural, and Computational Mapping to Define the Structural “Fingerprints” of Heart-Specific Atrial Fibrillation Drivers in Human Heart Ex Vivo. J Am Heart Assoc. 2017;6:e005922. doi:10.1161/JAHA.117.005922
17. Li N, Csepe TA, Hansen BJ, Sul L V, Kalyanasundaram A, Zakharkin SO, Zhao J, Guha A, Van Wagoner DR, Kilic A, et al. Adenosine-Induced Atrial Fibrillation. Circulation. 2016;134:486–498. doi:10.1161/CIRCULATIONAHA.115.021165 [PubMed: 27462069]
18. Lou Q, Hansen BJ, Fedorenko O, Csepe TA, Kalyanasundaram A, Li N, Hage LT, Glukhov A V, Billman GE, Weiss R, et al. Upregulation of Adenosine A1 Receptors Facilitates Sinoatrial Node Dysfunction in Chronic Canine Heart Failure by Exacerbating Nodal Conduction Abnormalities Revealed by Novel Dual-Sided Intramural Optical Mapping. Circulation. 2014;130:315–324. doi:10.1161/CIRCULATIONAHA.113.007086 [PubMed: 24838362]
19. Hansen BJ, Li N, Helfrich KM, Abudulwahed SH, Artiga EJ, Joseph ME, Mohler PJ, Hummel JD, Fedorov VV. First In Vivo Use of High-Resolution Near-Infrared Optical Mapping to Assess Atrial Activation During Sinus Rhythm and Atrial Fibrillation in a Large Animal Model. Circ Arrhythmia Electrophysiol. 2018;11:e006870. doi:10.1161/CIRCEP.118.006870
20. Le Guennec A, Malinowski S, Tavenard R. Data Augmentation for Time Series Classification using Convolutional Neural Networks. In: ECML/PKDD Workshop on Advanced Analytics and Learning on Temporal Data 2016 https://halshs.archives-ouvertes.fr/halshs-01357973
21. Dehghani A, Sarbishei O, Glatard T, Shihab E. A Quantitative Comparison of Overlapping and Non-Overlapping Sliding Windows for Human Activity Recognition Using Inertial Sensors. Sensors. 2019;19. doi:10.3390/s19225026
22. Cui Z, Chen W, Chen Y. Multi-Scale Convolutional Neural Networks for Time Series Classification. arXiv e-prints. Published online 2016:arXiv:1603.06995.
23. Hansen BJ, Zhao J, Fedorov VV. Fibrosis and Atrial Fibrillation: Computerized and Optical Mapping; A View into the Human Atria at Submillimeter Resolution. JACC Clin Electrophysiol. 2017;3:531–546. doi:10.1016/j.jacep.2017.05.002 [PubMed: 29159313]
24. Wolf M, Tavernier R, Zeidan Z, El Haddad M, Vandekerckhove Y, De Pooter J, Phlips T, Strisciuglio T, Almorad A, Kyriakopoulou M, et al. Identification of repetitive atrial activation patterns in persistent atrial fibrillation by direct contact high-density electrogram mapping. J Cardiovasc Electrophysiol. 2019;30:2704–2712. doi:10.1111/jce.14214 [PubMed: 31588635]
25. Dey D, Slomka PJ, Leeson P, Comaniciu D, Shrestha S, Sengupta PP, Marwick TH. Artificial Intelligence in Cardiovascular Imaging. J Am Coll Cardiol. 2019;73:1317–1335. doi:10.1016/j.jacc.2018.12.054 [PubMed: 30898208]
26. Krittanawong C, Johnson KW, Rosenson RS, Wang Z, Aydar M, Baber U, Min JK, Tang WHW, Halperin JL, Narayan SM. Deep learning for cardiovascular medicine: a practical primer. Eur Heart J. Published online 2019:1–15. doi:10.1093/eurheartj/ehz056 [PubMed: 30602013]
27. Price WN. Big data and black-box medical algorithms. Sci Transl Med. 2018;10:eaao5333. doi:10.1126/scitranslmed.aao5333
28. Sanders P, Berenfeld O, Hocini M, Jaïs P, Vaidyanathan R, Hsu L-F, Garrigue S, Takahashi Y, Rotter M, Sacher F, et al. Spectral analysis identifies sites of high-frequency activity maintaining

atrial fibrillation in humans. Circulation. 2005;112:789–797. doi:10.1161/CIRCULATIONAHA.104.517011 [PubMed: 16061740]

29. Kumagai K, Minami K, Sugai Y, Oshima S. Evaluation of the atrial substrate based on low-voltage areas and dominant frequencies after pulmonary vein isolation in nonparoxysmal atrial fibrillation. J arrhythmia. 2018;34:230–238. doi:10.1002/joa3.12049
30. Ramirez RJ, Takemoto Y, Martins RP, Filgueiras-Rama D, Ennis SR, Mironov S, Bhushal S, Deo M, Rajamani S, Berenfeld O, et al. Mechanisms by Which Ranolazine Terminates Paroxysmal but Not Persistent Atrial Fibrillation. Circ Arrhythmia Electrophysiol. 2019;12:e005557. doi:10.1161/CIRCEP.117.005557
31. Martins RP, Kaur K, Hwang E, Ramirez RJ, Willis BC, Filgueiras-Rama D, Ennis SR, Takemoto Y, Ponce-Balbuena D, Zarzoso M, et al. Dominant Frequency Increase Rate Predicts Transition from Paroxysmal to Long-Term Persistent Atrial Fibrillation. Circulation. 2014;129:1472–1482. doi:10.1161/CIRCULATIONAHA.113.004742 [PubMed: 24463369]
32. Quintanilla JG, Alfonso-Almazán JM, Pérez-Castellano N, Pandit S V, Jalife J, Pérez-Villacastín J, Filgueiras-Rama D. Instantaneous Amplitude and Frequency Modulations Detect the Footprint of Rotational Activity and Reveal Stable Driver Regions as Targets for Persistent Atrial Fibrillation Ablation. Circ Res. 2019;125:609–627. doi:10.1161/CIRCRESAHA.119.314930 [PubMed: 31366278]
33. Takahashi Y, O'Neill MD, Hocini M, Dubois R, Matsuo S, Knecht S, Mahapatra S, Lim KT, Jaïs P, Jonsson A, et al. Characterization of Electrograms Associated With Termination of Chronic Atrial Fibrillation by Catheter Ablation. J Am Coll Cardiol. 2008;51:1003–1010. doi:10.1016/j.jacc.2007.10.056 [PubMed: 18325439]
34. Gadenz L, Hashemi J, Shariat MH, Gula L, Redfearn DP. Clinical Role of Dominant Frequency Measurements in Atrial Fibrillation Ablation - A Systematic Review. J Atr Fibrillation. 2017;9:1548. doi:10.4022/jafib.1548 [PubMed: 29250291]
35. Jarman JWE, Wong T, Kojodjojo P, Spohr H, Davies JE, Roughton M, Francis DP, Kanagaratnam P, Markides V, Davies DW, et al. Spatiotemporal Behavior of High Dominant Frequency During Paroxysmal and Persistent Atrial Fibrillation in the Human Left Atrium. Circ Arrhythmia Electrophysiol. 2012;5:650–658. doi:10.1161/CIRCEP.111.967992
36. Elvan A, Linnenbank AC, van Bemmel MW, Misier ARR, Delnoy PPHM, Beukema WP, de Bakker JMT. Dominant frequency of atrial fibrillation correlates poorly with atrial fibrillation cycle length. Circ Arrhythm Electrophysiol. 2009;2:634–644. doi:10.1161/CIRCEP.108.843284 [PubMed: 19841032]
37. Roney CH, Cantwell CD, Bayer JD, Qureshi NA, Lim PB, Tweedy JH, Kanagaratnam P, Peters NS, Vigmond EJ, Ng FS. Spatial Resolution Requirements for Accurate Identification of Drivers of Atrial Fibrillation. Circ Arrhythm Electrophysiol. 2017;10:e004899-e004899. doi:10.1161/CIRCEP.116.004899

What Is Known?

- Persistent atrial fibrillation (AF) in humans can be maintained by localized reentrant drivers that requires personalized mapping for accurate locating and ablating for treatment.
- Identification of AF drivers by clinical multi-electrode mapping (MEM) is challenging due to primarily surface-only mapping and unvalidated interpretations of electrogram recordings.
- Subsurface high-resolution near-infrared optical mapping (NIOM) surpasses surface-only MEM due to its ability to properly resolve intramural conduction and detect AF drivers in the complex 3D structure of the human atria.

What this Study Adds?

- Simultaneous mapping of ex-vivo human atria with MEM and gold-standard NIOM can provide ground-truth labels for the supervised machine learning algorithm to efficiently classify MEM electrograms as AF driver or non-driver.
- Machine learning algorithms trained on Fourier spectra features of atrial electrograms may efficiently detect AF drivers and eventually guide targeted ablation.

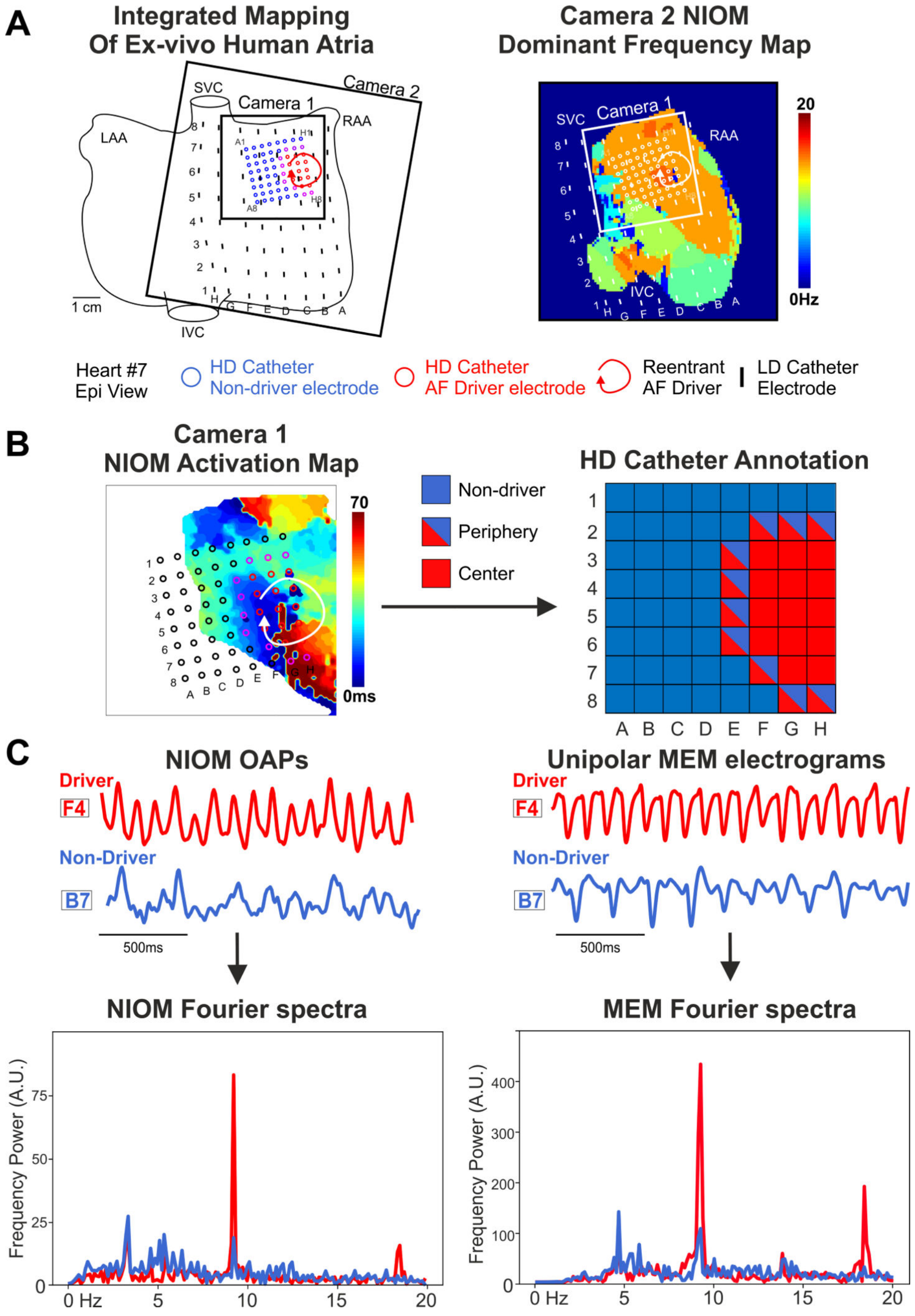

Figure 1.

Analytical Pipeline for Driver Prediction. (A) - Example of sustained AF episode maintained by reentrant driver, which was recorded simultaneously by clinical MEM (Higher-Density (HD) and Lower-Density (LD) catheters) and high-resolution NIOM (Cameras 1–2). (B) - Ground-truth labels for electrodes (red – center of driver, blue – non-driver) were acquired by NIOM, driver periphery labels (red/blue) were counted as driver in center plus periphery annotation or as non-driver in driver center annotation. (C) - Fourier spectra of annotated unipolar HD electrograms and co-located NIOM OAPs were used for generation of frequency features for Machine Learning approach. LAA/RAA = Left/Right Atria Appendage, I/SVC = Inferior/Superior Vena Cava, MEM = Multi-Electrode Mapping, NIOM = Near-Infrared Optical Mapping, OAP = Optical Action Potential, A.U. = Arbitrary Units.

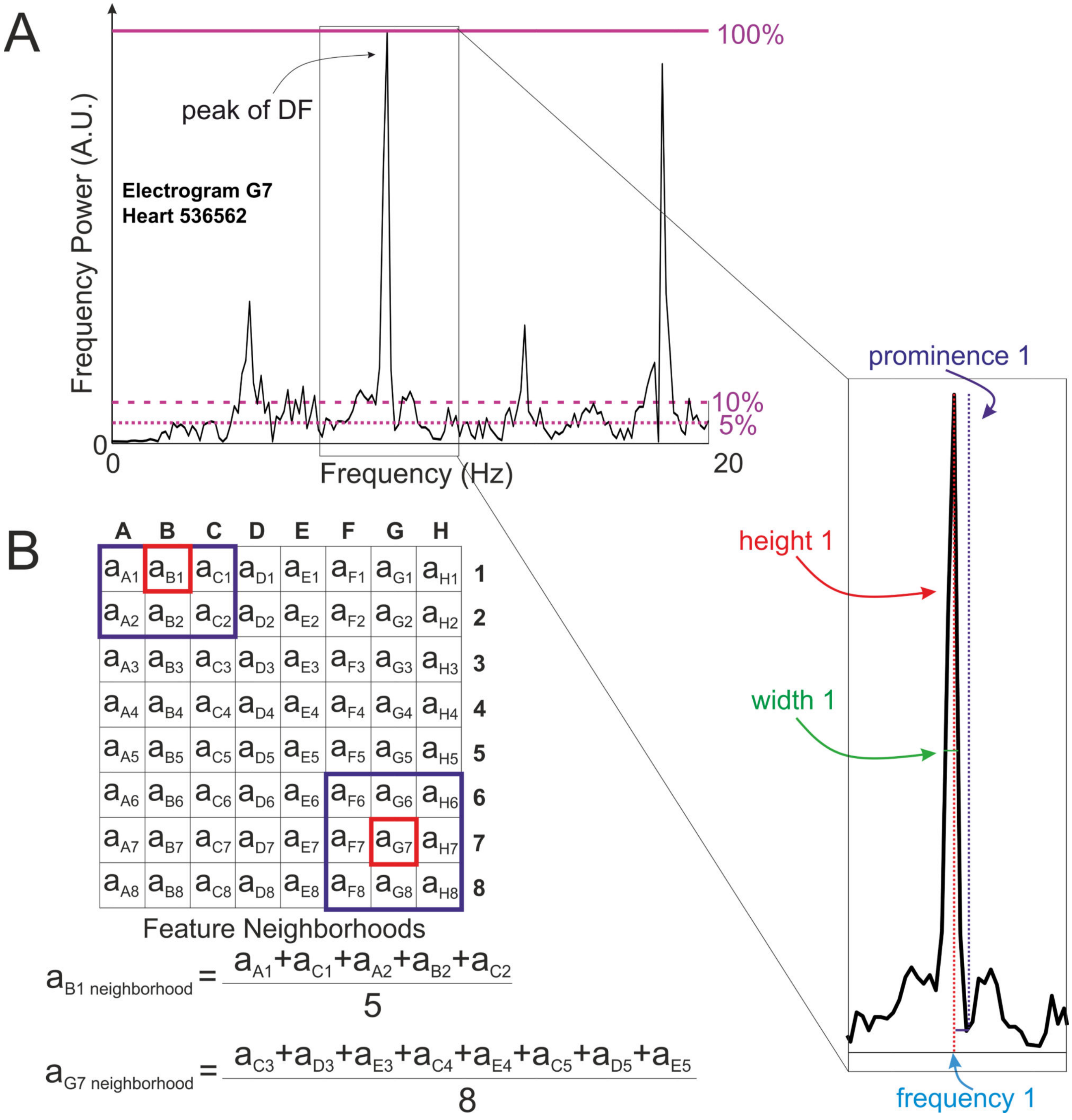

	A	B	C	D	E	F	G	H	
	a_{A1}	a_{B1}	a_{C1}	a_{D1}	a_{E1}	a_{F1}	a_{G1}	a_{H1}	1
	a_{A2}	a_{B2}	a_{C2}	a_{D2}	a_{E2}	a_{F2}	a_{G2}	a_{H2}	2
	a_{A3}	a_{B3}	a_{C3}	a_{D3}	a_{E3}	a_{F3}	a_{G3}	a_{H3}	3
	a_{A4}	a_{B4}	a_{C4}	a_{D4}	a_{E4}	a_{F4}	a_{G4}	a_{H4}	4
	a_{A5}	a_{B5}	a_{C5}	a_{D5}	a_{E5}	a_{F5}	a_{G5}	a_{H5}	5
	a_{A6}	a_{B6}	a_{C6}	a_{D6}	a_{E6}	a_{F6}	a_{G6}	a_{H6}	6
	a_{A7}	a_{B7}	a_{C7}	a_{D7}	a_{E7}	a_{F7}	a_{G7}	a_{H7}	7
	a_{A8}	a_{B8}	a_{C8}	a_{D8}	a_{E8}	a_{F8}	a_{G8}	a_{H8}	8

$$a_{B1\ \text{neighborhood}} = \frac{a_{A1}+a_{C1}+a_{A2}+a_{B2}+a_{C2}}{5}$$

$$a_{G7\ \text{neighborhood}} = \frac{a_{C3}+a_{D3}+a_{E3}+a_{C4}+a_{E4}+a_{C5}+a_{D5}+a_{E5}}{8}$$

Figure 2.

Features Calculation for Machine Learning Algorithm. (A) - Example of Fourier spectra for MEM recording with several of the 35 features labeled. The height of the highest peak (peak of DF) is indicated as purple line at 100%, the numbers of peaks above two thresholds of 5 and 10 % of the highest peak's height (dashed purple lines) were also used as features for Machine Learning algorithm. (B) - Calculation of the contribution of electrode neighborhood features at each electrode. DF = Dominant Frequency, A.U. = Arbitrary Units.

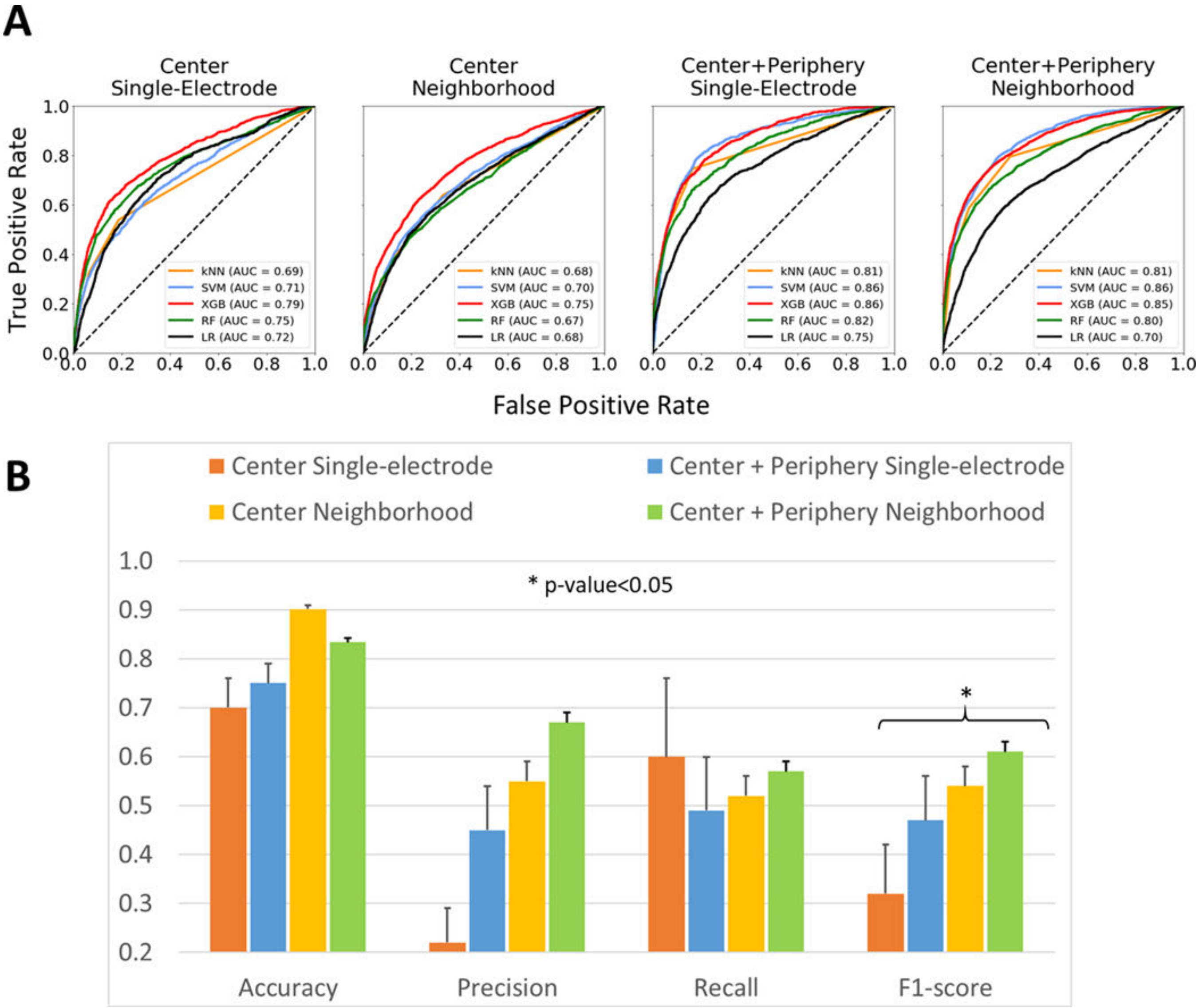

Figure 3.

Performance of Binary Classification. (A) - The Receiver Operating Characteristic (ROC) curves for different feature sets of AF dataset as analyzed by 5 algorithms. (B) - Performance metrics of kNN binary classification into AF reentrant driver vs non-driver recordings for different feature sets. Asterisk shows the significant difference between any two metrics within the group by ANOVA. MEM = Multi-Electrode Mapping, NIOM = Near-Infrared Optical Mapping. AUC = Area Under the Curve, kNN = k-Nearest Neighbors, SVM = Support Vector Machine, RF = Random Forest, XGB = XGBoost Classifier.

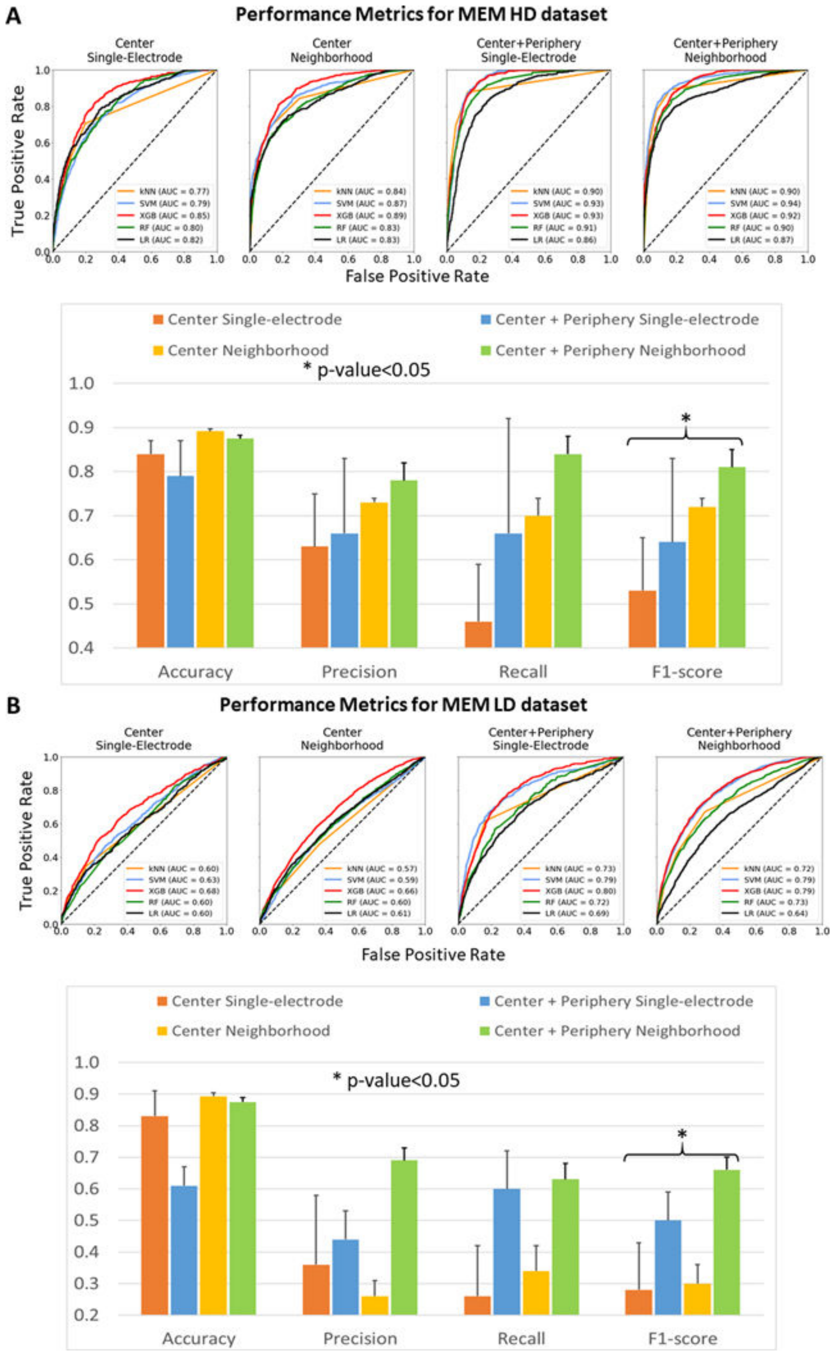

Figure 4.

Performance Metrics for HD and LD datasets. (A) - The ROC curves for different feature sets of AF HD dataset as analyzed by 5 algorithms. Below, performance metrics of binary classification into AF reentrant driver vs non-driver recordings from AF HD dataset for different feature sets. Asterisk shows the significant difference between any two metrics within group of three. (B) - The ROC curves for different feature sets of AF HD dataset as analyzed by 4 algorithms. Below, performance metrics of binary classification into AF reentrant driver vs non-driver recordings from AF LD dataset for different feature sets.

Asterisk shows the significant difference between any two metrics within the group by ANOVA. Abbreviations as in Figure 3, LD = Lower-Density catheter, HD = Higher-Density catheter.

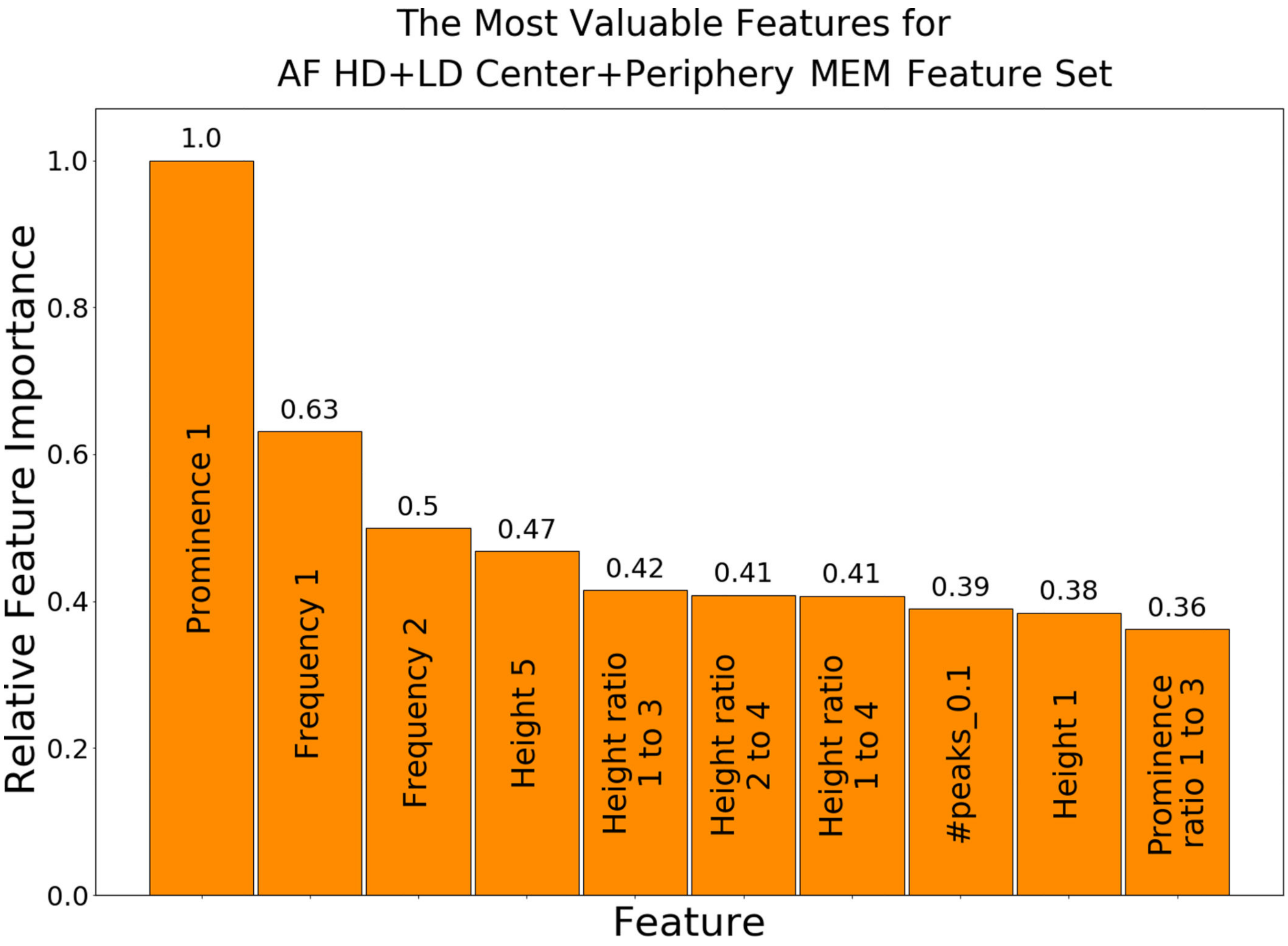

Figure 5.

The Most Valuable Features for Binary Classification. Relative feature importance of the top 10 most valuable features for neighborhood-electrodes MEM feature sets. Abbreviations as in Figure 1, PSDR - peak-to-standard deviation ratio.

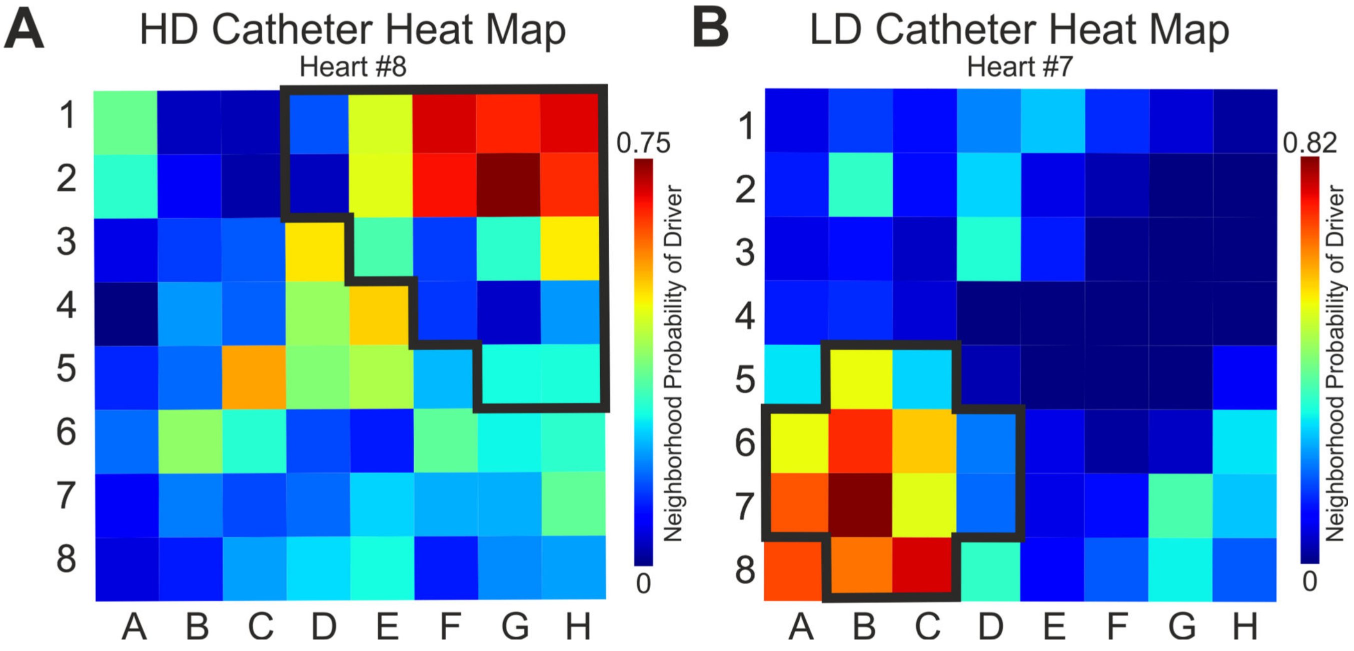

Figure 6.

Driver Prediction on 64 Electrodes Catheters. Examples of the Machine Learning probability prediction heat maps for two 64-electrode catheters - (A) Higher-density (HD) catheter and (B) Lower-density (LD) catheter. Ground truth driver region (center plus periphery) is outlined by black bold line. The color bar encodes probability of an electrode to be a driver.

Table 1.

Human heart mapping approaches.

Heart #	Preparation	MEM	NIOM	Sample numbers	Driver
1	Biatrial	LD	Epi	LD_1	1
2	LRA	LD	Epi/Endo	LD_2, LD_3	1
		LD	Epi/Endo	LD_4, LD_5	2
3	LRA	LD	Endo	LD_6	1
		LD	Epi/Endo	LD_7, LD_8	1
4	LRA	LD	Endo	LD_9	1
5	LRA	LD	Epi/Endo	LD_10, LD_11	1
		LD	Epi/Endo	LD_12, LD_13	1
		LD	Epi/Endo	LD_14, LD_15	2
		LD	Epi/Endo	LD_16, LD_17	1
6	LRA	LD	Epi/Endo	LD_18, LD_19	1
		LD	Epi/Endo	LD_20, LD_21	1
7	Biatrial	HD/LD	Endo	HD_1, LD_22	1
		HD/LD	Endo	HD_2, LD_23	1
8	Biatrial	HD/LD	Endo	HD_3, LD_24	1
9	Biatrial	LD	Endo	LD_25	1
10	Biatrial	HD	Epi	HD_4	1
11	Biatrial	HD	Epi	HD_5	1
		HD	Epi	HD_6	1
		HD	Epi	HD_7	2

LD = Lower-Density catheter, HD = Higher-Density catheter, Epi = Epicardial, Endo = Endocardial, LRA = Lateral Right Atrium, NIOM = Near-infrared optical mapping

Table 2.

Number of spectra from different datasets and modalities.

Dataset with Atrial Fibrillation (AF)	Lower-Density (LD) catheter	Higher-Density (HD) catheter	Combination
Number of MEM recordings	1600 (17%, 8%)	448 (27%, 9%)	2048 (20%, 7%)
Number of MEM spectra	17875 (19%, 0%)	8919 (33%, 0%)	26794 (23%, 0%)
Number of NIOM recordings	602 (32%, 6%)	448 (21%, 9%)	1050 (30%, 4%)
Number of NIOM spectra	6936 (34%, 0%)	8919 (32%, 0%)	15855 (33%, 0%)

The percentage of center plus periphery drivers and uninformative electrodes indicated in parentheses, respectively.

Table 3.

Names of features from MEM feature set.

#	Feature	#	Feature
1	#peaks_0.05	27	height ratio between peaks 2 and 3
2	#peaks_0.1	28	height ratio between peaks 2 and 4
3–7	frequency 1–5	29	height ratio between peaks 3 and 4
8–12	height 1–5	30	prominence ratio between peaks 1 and 2
13–17	width 1–5	31	prominence ratio between peaks 1 and 3
18–22	prominence 1–5	32	prominence ratio between peaks 1 and 4
23	PSDR	33	prominence ratio between peaks 2 and 3
24	height ratio between peaks 1 and 2	34	prominence ratio between peaks 2 and 4
25	height ratio between peaks 1 and 3	35	prominence ratio between peaks 3 and 4
26	height ratio between peaks 1 and 4		

MEM = Multi-Electrode Mapping, PSDR - peak-to-standard deviation ratio.